RSC Advances




ROYAL SOCIETY OF CHEMISTRY

www.rsc.org/advances

# Controlled *in-situ* synthesis of graphene oxide/zeolitic imidazolate frameworks composites with enhanced $CO_2$ uptake capacity

Binling Chen, Yanqiu Zhu and Yongde Xia*

College of Engineering, Mathematics and Physical Sciences, University of Exeter, Exeter EX4 4QF, United Kingdom.

E-mail: y.xia@exeter.ac.uk; Tel: +44 1392 723683.

**Abstract**

A simple and controlled in-situ synthesis method has been successfully used to produce graphene oxide/ZIF-8 composites from aqueous ammonia solution. A series of characterization techniques confirm the formation of strong interactions between ZIF-8 and graphene oxide in the synthesized composites. The crystal sizes of ZIF-8 and textual properties of composites can be tuned by the variable graphene oxide contents. The in-situ synthesized composites exhibit enhanced $CO_2$ adsorption energy and significant $CO_2$ uptake capacity due to the synergistic effect between graphene oxide and ZIF-8. The synergistic interactions of ZIFs and graphene oxide may offer a new approach to produce novel graphene oxide/ZIFs composites for diverse applications.

## 1 Introduction

Recently, a new sub-family of metal-organic frameworks (MOFs), zeolitic imidazolate frameworks (ZIFs), has attracted increasing attention. ZIFs are usually formed by a self-assembly approach and consist of M-Im-M bonds where M is Zn, Co and Im stands for imidazolate linker. Similar to traditional aluminosilicate zeolites, ZIFs possess diverse structures, where typically $M^{2+}$ ions play the role of silicon while the imidazolate anions form bridges that mimic the role of oxygen in zeolite frameworks, with the M-Im-M angle around $145^{o}$. Consequently, ZIFs are novel porous materials with ultrahigh surface area and exhibit unique crystal structures, abundant functionalities as well as exceptional thermal and chemical stabilities. This has triggered great interesting on their promising and potential applications in gas separation, catalysis, sensing and electronic devices, and drug delivery.[1-3] In particular, the presence of basic imidazolate units as an integral part of the frameworks offers great potential to utilize ZIFs as $CO_2$ capture candidates.[1, 4] However, owing to the relative small accessible pore apertures and/or the weak interactions between the pore walls and small gas molecules, it's difficult to fully take advantage of the ZIFs pores for gas adsorption. It is, nevertheless, suggested that the combination of an inert $CO_2$ absorbent with an active one, can produce a novel material that can remarkably improve $CO_2$ uptake efficiency.[5]

On the other hand, the last few years has witnessed the great risen interest in graphene and graphene-based materials.[6-8] Graphene oxide (GO), a very important precursor for graphene, has a layered structure with plenty of functional groups, which consist of hydroxyl and epoxy groups mostly into the graphene layers, and small amount of carboxy, carbonyl,

phenol, lactone and quinone on the edges of the layers.[9-12] GO is usually produced by chemical treatment of graphite with strong oxidizing agents. Owing to its unique structure, GO has been widely explored and utilized in the preparation of composite materials with promising adsorptive and electronic properties.[13-15]

Actually, MOFs-based graphite oxide composites have been investigated for various applications. For instance, Bandosz and colleagues reported the synthesis of MOF-5 and graphite oxide hybrid composites for the adsorption of ammonia;[15, 16] later they further explored the coordination chemistry of GO/MOF composites and their applications as adsorbents.[17] Recently, the same group found that the composites of copper-based MOF with aminated GO can enhance $CO_2$ adsorption.[18] Moreover, Jahan et al generated the conducting nanowires consisting of MOF-5 and functionalized graphene,[19] and they also prepared copper-centered MOFs and GO composite as a tri-functional catalyst in three important electrocatalysis reactions,[20] partly due to the good synergistic interactions between MOFs and GO. There are, however, rare reports on the ZIF/GO composites in literature. Recently, Rao and co-workers generated hybrid composites of GO with ZIF-8, which exhibited tunable nanoscale morphology and good $CO_2$ uptake at 195 K.[14] Unfortunately, the use of methanol as synthesis medium presents plenty of disadvantages, especially some environmental concerns since organic solvents are usually toxic and flammable. Moreover, the poor dispersion capacity of GO in methanol,[21] inevitably results in the formation of unhomogeneous samples such as mechanical mixtures that may remarkably decrease in the textural properties of the resulting materials. Therefore, these previous work encouraged us to explore a facile and green approach to generate graphene oxide/zeolitic imidazolate

frameworks composites that integrate the unique properties of both components. Herein, in this report, we present a simple and controllable *in-situ* synthesis method to produce GO/ZIF-8 composite materials in aqueous ammonia solution. These composites largely maintain the high textural properties, and the crystal sizes for ZIF-8 in the composites are tunable via control over the amount of GO in synthesis medium during the generation. The resulting GO/ZIF composites exhibited enhanced $CO_2$ uptake capacity due to the increased interactions between $CO_2$ molecules and the composites.

## 2 Experimental

### *2.1 Materials*

2-methylimidazole (99%, MIm), $Zn(NO_3)_2 \cdot 6H_2O$ (99%), 35 wt % ammonia solution, graphite power, $KMnO_4$ and 30% $H_2O_2$ were obtained from Sigma-Aldrich and used without further purification.

### *2.2 Materials synthesis*

#### *2.2.1 Synthesis of graphite oxide (GO)*

GO was prepared using a modified Hummers method.[22] Briefly, graphite powder (10 g) was mixed with concentrated $H_2SO_4$ (230 mL) under stirring and the temperature was controlled by an ice/water bath at 0 $^oC$, followed by the addition of $KMnO_4$ (30 g) slowly to the suspension and the reaction mixture was maintained at 2 $^oC$ under continuously stirring. After removal of the ice bath, the mixture was further stirred at room temperature for 0.5 hour. Oxidation of graphite occurred and very viscous dark brown product formed after 0.5 hour.

Distilled water (230 mL) was slowly added into the reaction vessel and the temperature was controlled at 98 $^{o}$C. The diluted suspension was stirred for an additional 15 minutes and further diluted with distilled water (1.4 L), before the addition of $H_2O_2$ (30%, 100 mL). The mixture was left overnight. GO particles, settled at the bottom, were separated from the excess liquid by decantation followed by centrifugation. The product was washed with plenty of distilled water for many cycles and separated by centrifugation till neutral pH is achieved. The solid product was transferred to petri dish and dried in air for further applications.

*2.2.2 Synthesis of GO/ZIF-8 composites*

Pure ZIF-8 was prepared from aqueous ammonia solution via a slight modified approach which was recently developed by our group.[23, 24] GO/ZIF-8 composites were also synthesized via the same method with slightly modification. Briefly, calculated amount of GO was dispersed in dilute aqueous ammonia solution and sonicated for 1 hour, followed by the addition of calculated amount of 2-methylimidazole (MIm) under stirring. This solution was then combined with a calculated amount of $Zn(NO_3)_2$ aqueous solution and was further stirred at room temperature for 24 hours. The molar ratio of synthesis mixture is $Zn^{2+}$ : MIm : $NH_3$ = 1 : 8 : 100. The product was collected after several water wash and centrifugation (6000 rpm for 10 minutes) cycles. Finally the power was air dried in a fume cupboard at room temperature. The resulting solid composites with variable GO content were denoted as xGO-ZIF, where x stands for the weight percentage of GO in comparison with ZIF-8. Therefore 3GO-ZIF, 10GO-ZIF, 15GO-ZIF, and 30GO-ZIF corresponds to the sample with weight ratio of GO to ZIF-8 in the composite is 3, 10, 15 and 30 wt%, respectively. A

mechanic mixing of GO and ZIF-8 with 10 wt% GO content, labelled as 10GO-ZIF-M, was also prepared for comparison.

*2.3 Materials characterization*

X-ray diffraction (XRD) patterns were recorded with Cu Kα radiation (40 kV-40 mA) at step time of 1 s and step size of 0.02 $^{o}$. Thermogravimetric analysis (TGA) / differential thermal analysis (DTA) was performed on a TA SDT Q600 instrument from room temperature to 800 $^{o}$C with a heating rate of 10 $^{o}$C min$^{-1}$ under a continuous air flow of 100 mL min$^{-1}$. A Hiden QGA gas analysis mass spectrometer (MS) was coupled with the TA SDT Q600 instrument to monitor and detect the gaseous compositions in the exhaust emission. Microscopy images of the samples were recorded using a Philips XL-30 scanning electron microscope (SEM) in a high vacuum mode and at an acceleration voltage of 20 kV. Samples were mounted using a conductive carbon double-sided sticky tape. A thin (*ca.* 10 nm) coating of gold was sputtered onto the samples to reduce the effects of charging. Transmission electron microscopy (TEM) images were obtained on a JOEL 2100 at an acceleration voltage of 100 kV. The samples were dispersed in absolute ethanol by moderate sonication at a concentration of 1 wt% solid for 30 minutes. The specimen was dispersed on a copper-supported carbon film. $N_2$ gas sorptions were carried out on a Quantachrome Autosorb-iQ gas sorptometer via conventional volumetric technique. Before gas analysis, the sample was evacuated for 4 h at 120 °C under vacuum. The textural properties were determined via nitrogen sorption at -196 °C. The surface area was calculated using the Brunauer-Emmett-Teller (BET) method based on adsorption data in the partial pressure (*P*/*P*o)

range of 0.02-0.22. The total pore volume was determined from the amount of nitrogen adsorbed at *P*/*P*o of ca. 0.99. Fourier-transform infrared (FTIR) spectra were obtained using an Alpha Bruker system. The samples were measured in the wavenumber range of 4000–450 $cm^{-1}$. The UV-Vis diffuse reflectance spectra were recorded on a UV-Vis spectrophotometer.

*2.4 $CO_2$ uptake measurement*

$CO_2$ gas adsorption capacities were carried out on a Quantachrome Autosorb-iQ gas sorptometer via conventional static volumetric technique. Prior to the gas adsorption analysis, the samples were evacuated for 5 h at 120 °C under vacuum. The $CO_2$ uptake capacities were performed at 0 and 25 °C.

## 3 Results and discussion

The X-ray diffraction patterns (XRD) of the controlled *in-situ* synthesized GO/ZIF-8 composites with different GO contents are presented in Fig. 1. For comparison, the XRD for pristine GO, bare ZIF-8 and a mechanical mixed sample 10GO-ZIF-M are also included in Fig. 1. The pristine GO shows a characteristic peak at 2θ of $12^{o}$, representing the average interlayer spacing of 7.4 Å;[25] while bare ZIF-8 exhibits pure sodalite (SOD)-type structures in the XRD patterns. Moreover, the mechanical mixed sample 10GO-ZIF-M displays XRD peaks contributed from both ZIF-8 and GO, suggesting that there is no obvious interaction between ZIF-8 and GO in the mechanical mixing sample. However, the XRD results of the controlled *in-situ* synthesized GO-ZIF composites exclusively exhibit only peaks from the sodalite (SOD)-type ZIF-8 without other new peaks or peaks from GO, regardless of GO

contents in the composites. Actually, even if the GO content is up to 30 wt%, the XRD patterns for the composite 30GO-ZIF (see ESI Fig. S1) are still similar to those for the ZIF-8 and other GO-ZIF composites with lower GO contents, indicating that GO sheets in the *in-situ* synthesized GO-ZIF composites may form strong interactions with ZIF-8 in the aqueous ammonia system during the synthesis procedure. Considering that GO contains rich hydroxyl, carboxy and epoxy groups, while 2-methylimidazole possesses abundant N-H functional groups, it is highly likely that the presence of GO may facilitate the formation of hydrogen bonds between GO and imidazolate unit that is an integral part of ZIF-8, resulting in the homogenously combination of imidazolate unit and GO, which is consistent with previous reports.[14] It is, however, worth noting that the XRD results of composites with higher GO contents are different from the previous reports,[14, 16] likely due to the poor dispersion ability of GO in organic solvents synthesis medium, which results in the formation of mechanical mixed-like composites. In addition, the XRD peak for GO may shift in a wide range depending on the water content in the GO sheet layers, thus its peak may be overlapped with the XRD peaks of ZIF-8 although we cannot rule out the possibility that the low GO content in the in-situ synthesized GO-ZIF8 composites may be beyond the detection limit of XRD instrument.

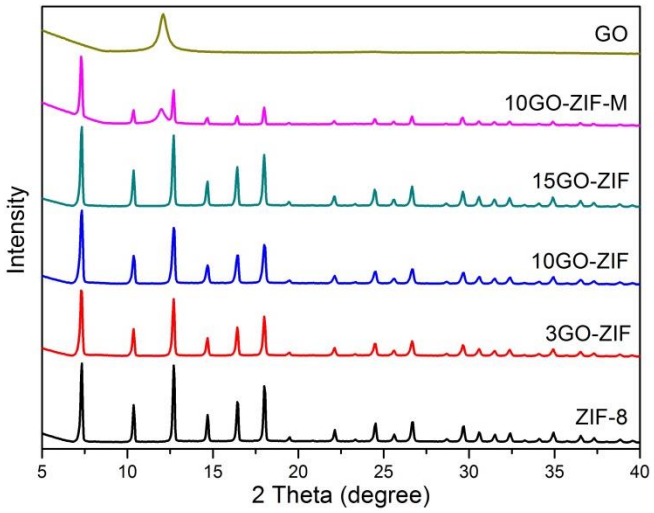

**Fig. 1** Powder XRD patterns of *in-situ* synthesized GO-ZIF composites, GO-ZIF-M, GO and ZIF-8.

The thermal gravimetric analysis (TGA) and corresponding mass spectroscopy (MS) signals of ZIF-8, 10GO-ZIF, 10GO-ZIF-M and pristine GO, performed under air flow were presented in Fig. 2, which provides another evidence of the formation of strong interaction between GO and ZIF-8 in the controlled *in-situ* synthesized GO-ZIF composites. For pristine GO, besides the removal of adsorbed water at low temperature (see the weight loss in Fig 2a and $H_2O$ signal in Fig 2d), it decomposes dramatically at 250 $^oC$, accompanied by the releasing of $CO_2$ and $H_2O$ (see Fig. 2a, b and d). For sample ZIF-8, two weight loss events centred at 450 and 500 $^oC$ were observed, corresponding to the decomposition of organic imidazolate species and the burning off the formed carbon species with the emission of $CO_2$, $NO_2$ and $H_2O$, as demonstrated by MS signals in Fig. 2b, c and d. For the mechanical mixed composite 10GO-ZIF-M, it exhibits not only the weight loss events in TGA but also the MS signals from both components GO and ZIF-8, implying that there is no obvious interaction between GO and ZIF-8 in this mechanically mixed sample. However, the TGA-MS results of the *in-situ* synthesized 10GO-ZIF composite exhibit similar decomposition temperatures, weight losses and gas releasing signals with the pristine ZIF-8, without any feature of pristine GO, indicating that the GO sheets in the *in-situ* synthesized composites may form strong interaction with ZIF-8, which is also in agreement with XRD results.

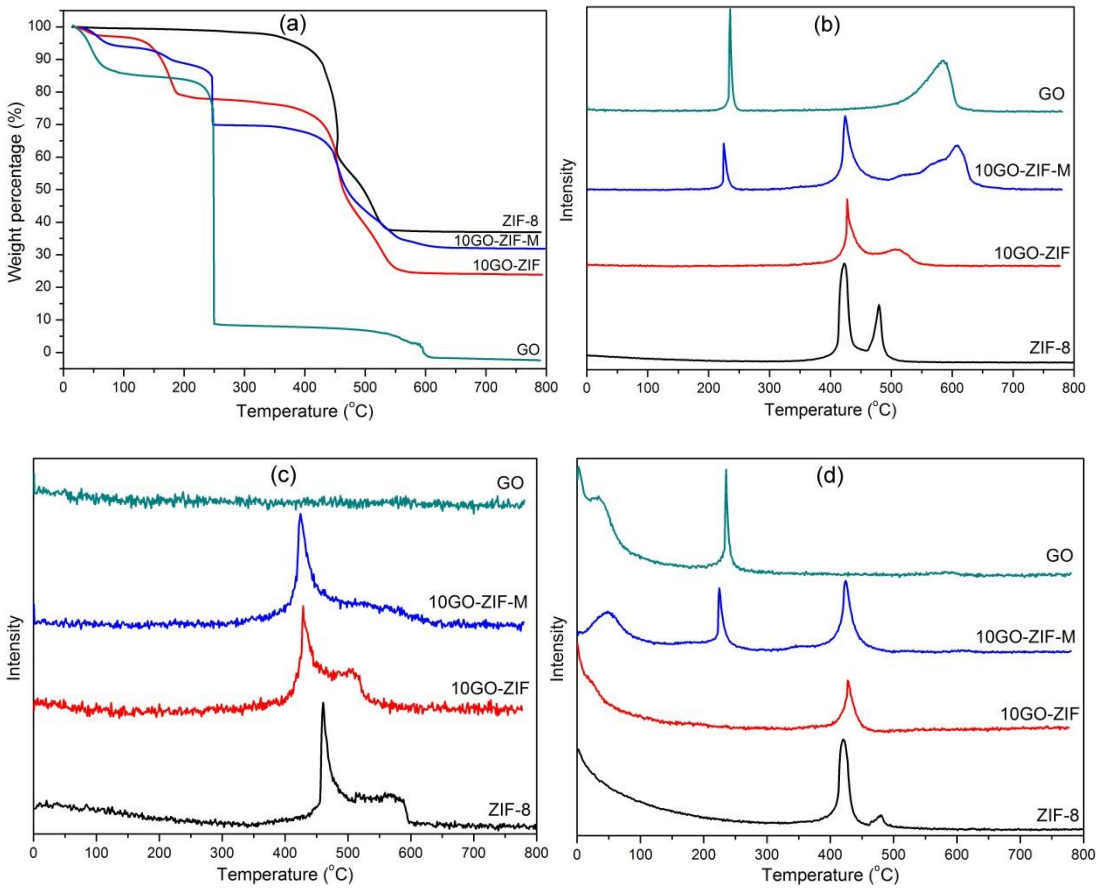


**Fig. 2** (a) TGA curves and MS signals of (b) $CO_2$, (c) $NO_2$ and (d) $H_2O$ respectively for sample GO, ZIF-8, 10GO-ZIF and 10GO-ZIF-M heated in air atmosphere.

Moreover, the FTIR spectra also confirm the formation of strong interaction between GO and ZIF-8 in the *in-situ* synthesized GO-ZIF composites. As shown in Fig. 3a, all the *in-situ* synthesized GO-ZIF composites exclusively exhibit FTIR spectra similar to ZIF-8, but the mechanical mixed 10GO-ZIF-M sample displays spectrum contributed from both GO and ZIF-8. As presented in Fig. 3b, most of the absorption bands for ZIF-8 and the *in-situ* synthesized GO/ZIF composites are associated with the vibrations of the imidazole units, such as the peak at 1584 $cm^{-1}$ can be assigned as the C=N stretch mode, while the bands at 1350–1500 $cm^{-1}$ are associated with the imidazole ring stretching. The bands in the spectral regions

of 900–1350 $cm^{-1}$ and those below 800 $cm^{-1}$ are assigned as the in-plane bending and out-of-plane bending of the imidazole ring.[26] Particularly, the strong bands at 1150 and 995 $cm^{-1}$ is due to the C-N stretching of the imidazole units. Clearly, no bands can be attributed to C-O bonds in the *in-situ* synthesized GO-ZIF composites. However, the mechanical mixed 10GO-ZIF-M sample displays absorption bands not only from ZIF-8, but also the main bands from GO, such as C=O stretching vibrations at 1710 $cm^{-1}$, C-O stretching vibrations in epoxy or alkoxy groups at 1049 $cm^{-1}$ and C=C skeletal vibration bands from unoxidized graphitic domains or the stretching deformation vibration of intercalated water at 1620 $cm^{-1}$, which are consistent with previous reports.[27] These observations clearly confirmed that strong interactions are formed between GO and ZIF-8 in the *in-situ* synthesized GO-ZIF composites, while no such interactions exist in the mechanical mixed 10GO-ZIF-M sample.

Fig. 4 presents the UV-Vis absorption spectra of GO, ZIF-8 and 10GO-ZIF dispersed in water. The absorption peak of GO at 217 nm is due to the characteristic $\pi$ – plasmon absorption and a shoulder peak at about 260 nm, which is assigned to $n-\pi$ transitions of C=O bonds. The pristine ZIF-8 has an absorption band at 220 nm, while 10GO-ZIF composite shows a slight shift in absorption band at 222 nm compared to pristine ZIF-8. This red shift in the absorption band could be caused by charge or energy transfer interaction between the poly-aromatic scaffold in GO and ZIF-8,[20] further suggesting the formation of strong interaction between the GO and ZIF-8 species in the *in-situ* synthesized GO/ZIF composites.

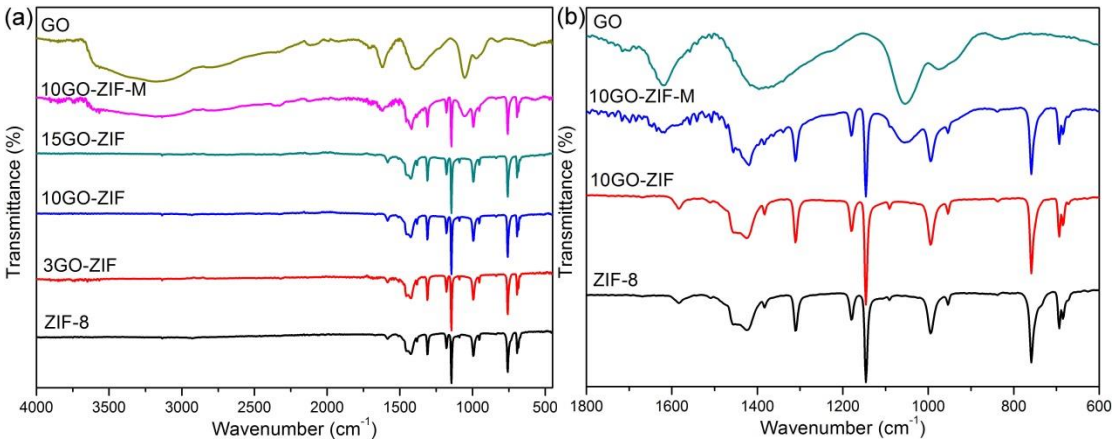


**Fig. 3** FTIR spectra of GO-ZIF composites, GO-ZIF-M, GO and ZIF-8.

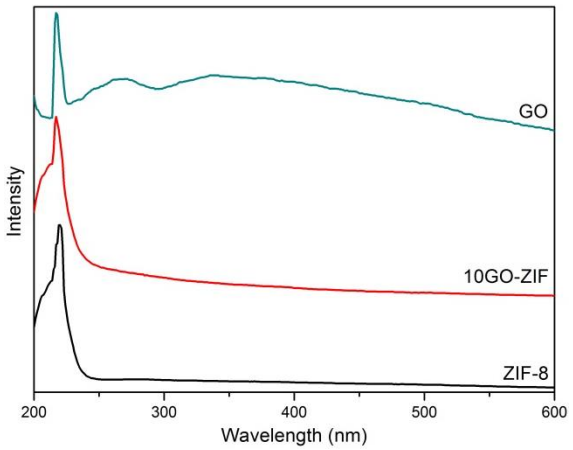


**Fig. 4** UV-Vis spectra of GO, ZIF-8 and representative GO-ZIF composite.

The morphologies of the studied samples were characterized using scanning electron microscopy (SEM) and transmission electron microscopy (TEM). SEM images in Fig. 5a-d show that the pristine ZIF-8 crystals have the uniform micrometer-sized cubic shapes, which is consistent with previous report.[28] Obviously, the crystal size of ZIF-8 can be adjustable by control over the amount of GO in the *in-situ* synthesized composites. The average crystal size for ZIF-8 particles decreases gradually from 5 μm for pristine ZIF-8 to 1.5 μm for *in-situ* synthesized 15GO-ZIF sample with 15 wt% GO content. Actually, if the GO content in the

*in-situ* synthesized composite further increases up to 30 wt%, the average crystal size for ZIF-8 particles in the resulting 30GO-ZIF sample can decrease to 0.7 μm (see ESI Fig. S2). The crystal sizes of ZIF-8 particles in the *in-situ* synthesized GO-ZIF composites are probably controlled by the functional groups of GO through coordination modulation which inhibits the growth of crystals,[14] in which the GO sheets could be performed as a structure-directing agent for the nucleation and growth of ZIF-8 crystals. In addition, Fig. 5e and 5f present the SEM images of 10GO-ZIF-M and GO, respectively. Obviously, the mechanical mixed sample 10GO-ZIF-M displays ZIF-8 crystals with size around 5 μm and the GO sheets are clearly separated from the ZIF-8 crystal without any interactions with GO due to mechanical mixing.

Representative TEM images of *in-situ* synthesized 10GO-ZIF composite were presented in Fig. 6. It is found that the as-synthesized GO-ZIF composite exhibits the regular cubic-shape of ZIF-8 crystals, which is consistent with the SEM results. Furthermore, it can be clearly observed that some GO sheets are attached on the edges of the ZIF-8 crystals (Fig. 6a) and some GO sheets are actually embedded in the ZIF-8 cubic particles (Fig. 6b), suggesting the potential to form strong interaction between the ZIF-8 particle and GO sheets; Consequently, it's likely to generate homogenously ordered structures in the *in-situ* synthesized GO-ZIF composites.[16] However, it's worth noting that the particle sizes for GO in the in-situ synthesized GO-ZIF8 composites (Fig 6a) are much smaller than those for pristine GO (Fig 5f), which also further confirm that the GO in the *in-situ* synthesized GO-ZIF8 composites is different from the pristine GO particles due to the formation of new chemical bonds between GO and ZIFs crystals.

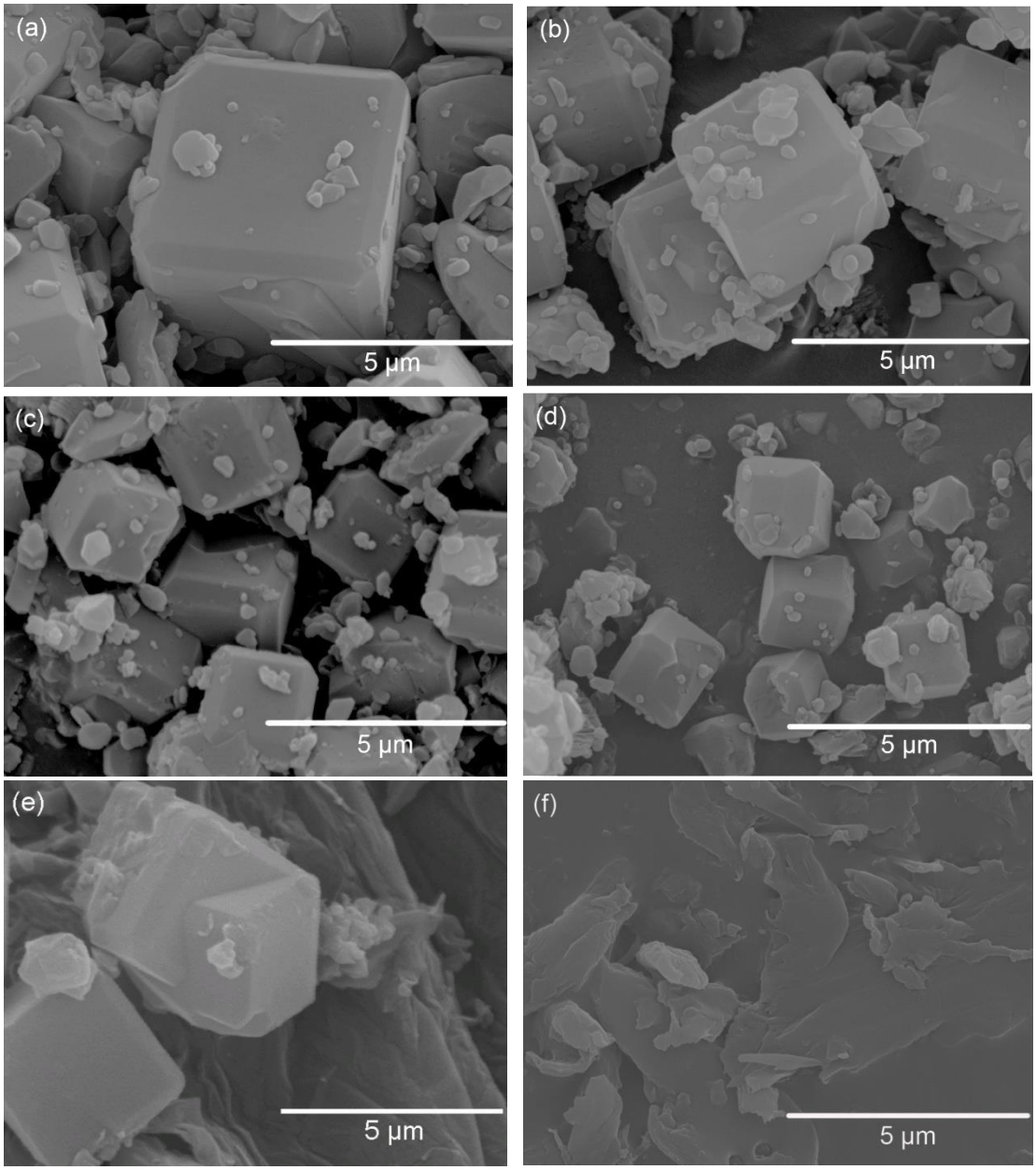


**Fig. 5** Representative SEM images of *in-situ* synthesized GO-ZIF composites and GO sample: (a) ZIF-8, (b) 3GO-ZIF, (c) 10GO-ZIF, (d) 15GO-ZIF, (e) 10GO-ZIF-M and (f) GO.

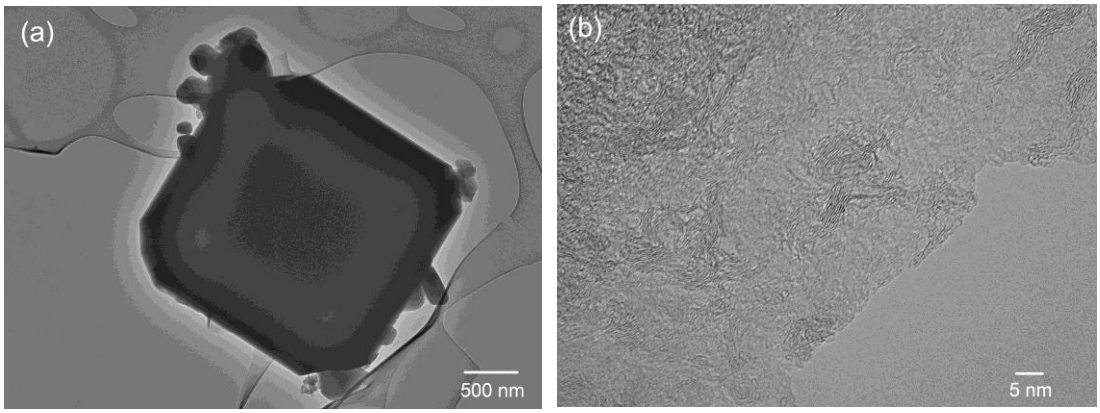


**Fig. 6** Representative TEM images of *in-situ* synthesized 10GO-ZIF composite.

The textural properties of the GO-ZIF composites can be obtained from $N_2$ adsorption–desorption measurements at liquid nitrogen temperature. As shown in Fig. 7, the nitrogen sorption for GO is quite low because of its nonporous structure,[29] and all the *in-situ* as-synthesized GO-ZIF composites show type I isotherms with adsorption and desorption branches are completely reversible, indicating negligible mesopores existed in these composites. Moreover, all the *in-situ* synthesized GO-ZIF composites display significant adsorption of nitrogen under low relative pressure, implying those composites are micropore dominated materials, which are in agreement with the microporous nature of ZIF-8 material (as shown in Fig. 7). The mechanical mixed sample 10GO-ZIF-M also exhibits large quantity of nitrogen adsorption under low relative pressure in its isotherms due to the microporous nature of ZIF-8; however, it shows a large hysteresis loop between adsorption and desorption branches, suggesting the existence of mesoporous voids between the sample particles, which is obviously different from the *in-situ* synthesized GO-ZIF composites. In addition, as summarized in Table 1, the textual properties of the *in-situ* synthesized GO-ZIF composites are tunable by control over the GO content in the composites. Generally, compared to the

pristine ZIF-8, the surface area and pore volume for the *in-situ* synthesized GO-ZIF composites with lower GO content (such as sample 3GO-ZIF and 10GO-ZIF) increase slightly, but the surface area for GO-ZIF composite with higher GO content (such as sample 15GO-ZIF) decreases slightly. The increase in surface area for lower GO content composites (sample 3GO-ZIF and 10GO-ZIF) can arise from the synergistic effect,[18] which is the strong interactions between GO and ZIF-8 resulting in the formation of new developed porosities in the *in-situ* synthesized composites; while the decrease in surface area for 15GO-ZIF may due to an increasing proportion of nonporous GO in the composite, which may result in partially blocking the pore channels of ZIF-8. Compared to the pristine ZIF-8, the *in-situ* synthesized 15GO-ZIF composite with 15 wt% GO exhibits small level (around 5.6%) of decrease in surface area. On the contrary, a mechanical mixed sample 10GO-ZIF-M with 10 wt% GO, shows surface area of 1188 $m^2$ $g^{-1}$, which is 15.6% lower than that of the pristine ZIF-8 sample and 16.0% lower than that of *in-situ* synthesized 10GO-ZIF composite with the same amount of GO content. These observations clearly demonstrated that the *in-situ* synthesized composites are not just simply a physical mixture of GO and ZIF-8, but formed by a synergy effect between GO and ZIF-8. This synergistic effect may not only lead to form new porosity between GO and ZIF-8 units, but also may cause those "lace-like" structures where GO sheets could be embedded within ZIF-8 crystals.[18]

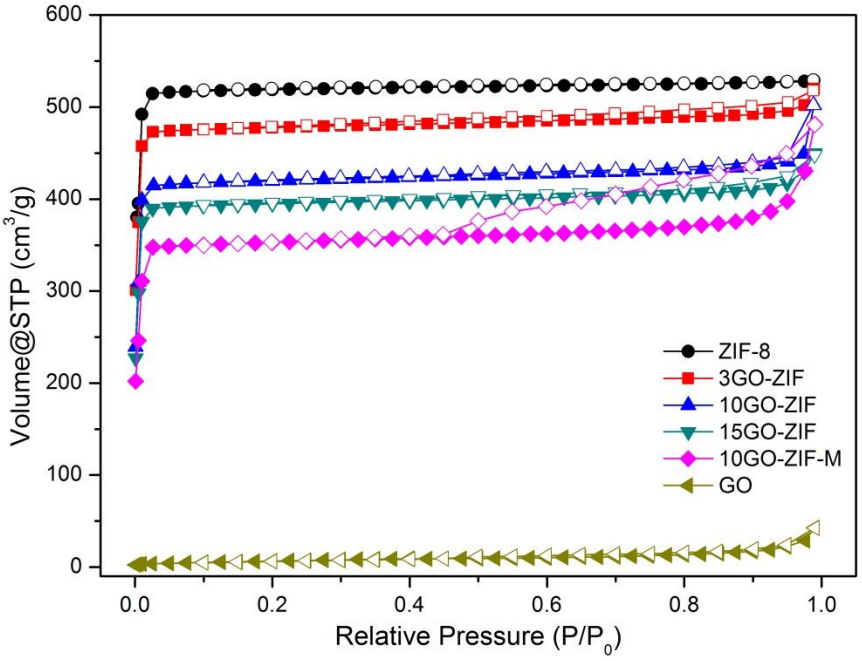


**Fig. 7** Nitrogen sorption isotherms measured at -196 $^{o}$C for sample GO, ZIF-8, 10GO-ZIF-M and the as-synthesized composites (3GO-ZIF, 10GO-ZIF and 15GO-ZIF). For clarity, the isotherms for samples 3GO-ZIF and ZIF-8 are offset for 50 and 100 along y axis respectively.

**Table 1** Textural properties and $CO_2$ uptake capacities of studied samples.

| Sample | GO content (wt %) | Surface area ($m^2$ $g^{-1}$) | Pore volume ($cm^3$ $g^{-1}$) | $CO_2$ uptake at 1.0 bar ($cm^3$ $g^{-1}$) |
|---|---|---|---|---|
| ZIF-8 | 0 | 1408 | 0.67 | 37 |
| 3GO-ZIF | 3 | 1439 | 0.71 | 40 |
| 10GO-ZIF | 10 | 1414 | 0.78 | 49 |
| 15GO-ZIF | 15 | 1328 | 0.68 | 35 |
| 10GO-ZIF-M | 10 | 1188 | 0.74 | 33 |
| GO | 100 | 25 | 0.07 | 6 |

A variety of porous materials including zeolites, mesoporous silicas, MOFs and porous

carbons can be used as solid adsorbents for $CO_2$ capture due to the increased environmental concerns.[30-33] The $CO_2$ adsorption capacities at 0 $^oC$ for GO, ZIF-8, 10GO-ZIF-M and the *in-situ* synthesized composites (3GO-ZIF, 10GO-ZIF and 15GO-ZIF) are presented in Fig. 8a and their $CO_2$ uptake capacities are also summarized in Table 1. Generally, $CO_2$ uptake capacities of porous materials are related to samples surface area, which is consistent with our previous report.[34] GO is a weak $CO_2$ adsorbent with an uptake capacity of 6 $cm^3$ $g^{-1}$ at 0 $^oC$ and 1.0 bar, while the pristine ZIF-8 shows a $CO_2$ uptake capacity of 37 $cm^3$ $g^{-1}$ under the same conditions. Compared with the pristine ZIF-8, the *in-situ* synthesized composites with GO content up to 10 wt% (sample 3GO-ZIF and 10GO-ZIF) exhibit increased $CO_2$ uptake capacities, but the composite with higher GO content (sample 15GO-ZIF) then shows decreased $CO_2$ adsorption. As a result, both samples 3GO-ZIF and 10GO-ZIF display higher $CO_2$ uptake while sample 15GO-ZIF show slightly lower $CO_2$ sorption capacity than pristine ZIF-8. It is worth noting that compared with the pristine ZIF-8, the *in-situ* synthesized 10GO-ZIF composite exhibited up to 33% increase in the $CO_2$ uptake capacity at 0 $^oC$ and 1.0 bar. This unusual $CO_2$ uptake can also be attributed to the synergistic effect of GO and ZIF-8, where GO with different functional groups provides specific interaction sites for $CO_2$.[14] Moreover, the formation of hydrogen bonds between GO and imidazolate unit that is an integral part of ZIF-8 can increase not only the degree of interaction between graphene oxide layers and ZIF-8 crystals, but also the generation of new porosities. Consequently, the total porosities of the composites have been increased and therefore the $CO_2$ adsorption capacities have also been enhanced. This is supported by the data in Table 1 where the $CO_2$ uptake capacity of sample 10GO-ZIF is higher than that of pristine ZIF-8 and bare GO. In

addition, as the composites were synthesized in aqueous ammonia solution medium, the synthesized composites may undergo N-doping treatment, which may benefit to $CO_2$ adsorption.[35] However, the mechanical mixed sample 10GO-ZIF-M shows $CO_2$ uptake capacity of 33 $cm^3$ $g^{-1}$, which is 10.8% and 32.7% lower than that of pristine ZIF-8 and *in-situ* synthesized 10GO-ZIF composite with the same amount of GO content respectively. Therefore, the introduction of GO into the composites via controlled *in-situ* synthesized method can effectively affect the textural properties and consequently influence remarkably on the $CO_2$ uptake capacities of resulting composites.

The $CO_2$ adsorption energy (i.e., isosteric heat of adsorption, $Q_{st}$), which indicates the strength of interaction between $CO_2$ molecules and the adsorbents, was calculated using the $CO_2$ sorption isotherms measured at 0 and 25 $^oC$ based on the Clausius–Clapeyron equation. The plots of $Q_{st}$ as a function of $CO_2$ uptake for ZIF-8 and 10GO-ZIF are presented in Fig. 8b. The initial isosteric heat of the adsorption $Q_{st}$ for pristine ZIF-8 is 32 kJ $mol^{-1}$ at low $CO_2$ uptake (low surface coverages), which gradually drops to an average $Q_{st}$ of 29 kJ $mol^{-1}$ at high $CO_2$ uptake (high surface coverages). The initial and average $Q_{st}$ for ZIF-8 are generally higher than those values reported in literature[14, 36] These observed higher $Q_{st}$ values for ZIF-8 are probably due to the use of the aqueous ammonia solution as synthesis system. Interestingly, the initial isosteric heat of the adsorption $Q_{st}$ for the representative *in-situ* synthesized 10GO-ZIF composite displays a significant high value of 50 kJ $mol^{-1}$ at low $CO_2$ uptake, suggesting a strong interaction between $CO_2$ molecule and 10GO-ZIF composite. It indicated that under aqueous ammonia system, the synergistic effect of GO and ZIF-8 plays a predominant role in the initial interaction when $CO_2$ adsorbed on the surface of the composite,

probably due to the formation of strong acid-base interaction between the acidic $CO_2$ molecules and the basic imidazolate units as an integral part of the composites. At higher $CO_2$ coverages, the $Q_{st}$ value of 10GO-ZIF reduces to an average value of 31 kJ $mol^{-1}$, which is higher than that of ZIF-8, suggesting stronger interaction between $CO_2$ molecule and the *in-situ* synthesized 10GO-ZIF than that in ZIF-8 at higher $CO_2$ coverages, due to the synergistic effect between GO and ZIF in the *in-situ* synthesized 10GO-ZIF composite. The synergistic interactions of ZIFs and GO may offer a new approach to prepare other ZIFs/GO composites for different applications.

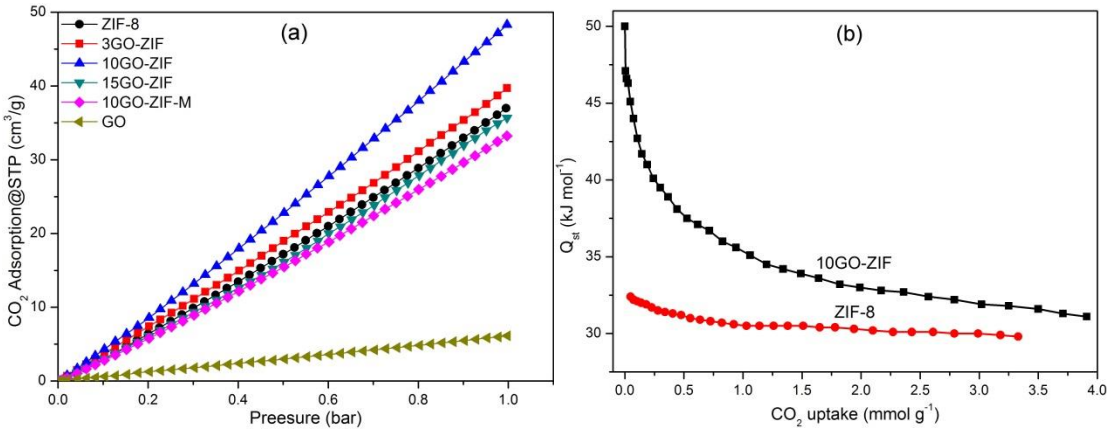


**Fig. 8** (a) $CO_2$ adsorption capacities at 0 $^oC$ for sample GO, ZIF-8, 10GO-ZIF-M and the *in-situ* synthesized composites (3GO-ZIF, 10GO-ZIF and 15GO-ZIF); (b) Isosteric heat of $CO_2$ adsorption ($Q_{st}$) for representative *in-situ* synthesized 10GO-ZIF composite and pure ZIF-8 as a function of the amount of $CO_2$ adsorbed.

## 4 Conclusions

To conclude, composites containing ZIF-8 and various contents of GO have been successfully prepared using an *in-situ* controlled synthesis method in aqueous ammonia

system. Different material characterization techniques including XRD, TGA-MS, FTIR and UV-Vis spectra confirm the formation of strong interactions between ZIF-8 and GO in the synthesized composites. The crystal sizes of ZIF-8 and the textural properties of composites can be modulated by the control over the amount of GO in the composites. GO may act as a potential structure-directing agent for the growth and stabilization of ZIF-8 crystals. In addition, the *in-situ* synthesized composites show enhanced $CO_2$ adsorption energy and significant $CO_2$ storage capacity, due to the strong interactions and the synergistic effect between GO and ZIF-8 facilitating the formation of new developed porosities in the *in-situ* synthesized composites. The synergistic interactions of ZIFs and GO may provide a new path to fabricate novel GO/ZIFs composites for a wide range of applications.

## Acknowledgement

The financial support by the Royal Society, the Royal Academy of Engineering and University of Exeter is greatly acknowledged.

## References


1. A. Phan, C. J. Doonan, F. J. Uribe-Romo, C. B. Knobler, M. O'Keeffe and O. M. Yaghi, *Acc. Chem. Res.*, 2009, **43**, 58-67.
2. J. Yao and H. Wang, *Chem. Soc. Rev.*, 2014, **43**, 4470-4493.
3. B. Chen, Z. Yang, Y. Zhu and Y. Xia, *J. Mater. Chem. A*, 2014, **2**, 16811-16831.
4. J.-P. Zhang, A.-X. Zhu, R.-B. Lin, X.-L. Qi and X.-M. Chen, *Adv. Mater.*, 2011, **23**, 1268-1271.
5. D. Liu, J. Gu, Q. Liu, Y. Tan, Z. Li, W. Zhang, Y. Su, W. Li, A. Cui, C. Gu and D. Zhang, *Adv. Mater.*, 2014, **26**, 1229-1234.
6. S. Stankovich, D. A. Dikin, G. H. B. Dommett, K. M. Kohlhaas, E. J. Zimney, E. A. Stach, R. D. Piner, S. T. Nguyen and R. S. Ruoff, *Nature*, 2006, **442**, 282-286.
7. D. A. Dikin, S. Stankovich, E. J. Zimney, R. D. Piner, G. H. B. Dommett, G. Evmenenko, S. T. Nguyen and R. S. Ruoff, *Nature*, 2007, **448**, 457-460.
8. S. Stankovich, D. A. Dikin, R. D. Piner, K. A. Kohlhaas, A. Kleinhammes, Y. Jia, Y. Wu, S. T. Nguyen and R. S. Ruoff, *Carbon*, 2007, **45**, 1558-1565.
9. D. Chen, H. Feng and J. Li, *Chem. Rev.*, 2012, **112**, 6027-6053.
10. G. Eda and M. Chhowalla, *Adv. Mater.*, 2010, **22**, 2392-2415.
11. X. Li, G. Zhang, X. Bai, X. Sun, X. Wang, E. Wang and H. Dai, *Nature Nanotechn.*, 2008, **3**, 538-542.
12. F. Kim, L. J. Cote and J. Huang, *Adv. Mater.*, 2010, **22**, 1954-1958.
13. J. Li, L. Vaisman, G. Marom and J.-K. Kim, *Carbon*, 2007, **45**, 744-750.
14. R. Kumar, K. Jayaramulu, T. K. Maji and C. N. Rao, *Chem. Commun.*, 2013, **49**,

4947-4949.

15. C. Petit and T. J. Bandosz, *Adv. Funct. Mater.*, 2010, **20**, 111-118.
16. C. Petit and T. J. Bandosz, *Adv. Mater.*, 2009, 4753-4757.
17. C. Petit and T. J. Bandosz, *Dalton Trans.*, 2012, **41**, 4027-4035.
18. Y. X. Zhao, M. Seredych, Q. Zhong and T. J. Bandosz, *RSC Adv.*, 2013, **3**, 9932-9941.
19. M. Jahan, Q. Bao, J.-X. Yang and K. P. Loh, *J. Am. Chem. Soc.*, 2010, **132**, 14487-14495.
20. M. Jahan, Z. Liu and K. P. Loh, *Adv. Funct. Mater.*, 2013, **23**, 5363-5372.
21. D. R. Dreyer, S. Park, C. W. Bielawski and R. S. Ruoff, *Chem. Soc. Rev.*, 2010, **39**, 228-240.
22. W. S. Hummers and R. E. Offeman, *J. Am. Chem. Soc.*, 1958, **80**, 1339-1339.
23. B. Chen, F. Bai, Y. Zhu and Y. Xia, *Microporous Mesoporous Mater.*, 2014, **193**, 7-14.
24. B. Chen, F. Bai, Y. Zhu and Y. Xia, *RSC Adv.*, 2014, **4**, 47421-47428.
25. C. Hontoria-Lucas, A. J. López-Peinado, J. d. D. López-González, M. L. Rojas-Cervantes and R. M. Martín-Aranda, *Carbon*, 1995, **33**, 1585-1592.
26. Y. Hu, H. Kazemian, S. Rohani, Y. Huang and Y. Song, *Chem. Commun.*, 2011, **47**, 12694-12696.
27. Y. Xu, H. Bai, G. Lu, C. Li and G. Shi, *J. Am. Chem. Soc.*, 2008, **130**, 5856-5857.
28. M. He, J. Yao, Q. Liu, K. Wang, F. Chen and H. Wang, *Microporous Mesoporous Mater.*, 2014, **184**, 55-60.
29. M. Seredych, C. Petit, A. V. Tamashausky and T. J. Bandosz, *Carbon*, 2009, **47**, 445-456.

30. Q. Wang, J. Luo, Z. Zhong and A. Borgna, *Energy Environ. Sci.*, 2011, **4**, 42-55.

31. N. Gargiulo, F. Pepe and D. Caputo, *J. Nanosci. Nanotechnol.*, 2014, **14**, 1811-1822.

32. N. Gargiulo, A. Peluso, P. Aprea, F. Pepe and D. Caputo, *J. Chem. Eng. Data*, 2014, **59**, 896-902.

33. N. Gargiulo, F. Pepe and D. Caputo, *J. Colloid Interface. Sci.*, 2012, **367**, 348-354.

34. Y. Xia, R. Mokaya, G. S. Walker and Y. Zhu, *Adv. Energy Mater.*, 2011, **1**, 678-683.

35. F. Bai, Y. Xia, B. Chen, H. Su and Y. Zhu, *Carbon*, 2014, **79**, 213-226.

36. S. Gadipelli, W. Travis, W. Zhou and Z. X. Guo, *Energy Environ. Sci.*, 2014, **7**, 2232-2238.

## Table of Contents:

Novel GO-ZIF8 composites synthesized via controlled in-situ method exhibit enhanced $CO_2$ uptake capacity due to the synergistic effect.